# Wrinkles and splay conspire to give positive disclinations negative curvature

Elisabetta A. Matsumoto[a,b,1,2], Daniel A. Vega[c,1,2], Aldo D. Pezzutti[c], Nicolás A. García[c,3], Paul M. Chaikin[d], and Richard A. Register[e]

[a]Princeton Center for Theoretical Science, Princeton University, Princeton, NJ 08544; [b]John A. Paulson School of Engineering and Applied Sciences, Harvard University, Cambridge, MA 02138; [c]Instituto de Física del Sur, Consejo Nacional de Investigaciones Científicas y Técnicas, Universidad Nacional del Sur, 8000 Bahía Blanca, Argentina; [d]Center for Soft Condensed Matter Research and Department of Physics, New York University, New York, NY 10003; and [e]Department of Chemical and Biological Engineering and Princeton Institute for the Science and Technology of Materials, Princeton University, Princeton, NJ 08544

Edited by Monica Olvera de la Cruz, Northwestern University, Evanston, IL, and approved September 1, 2015 (received for review July 21, 2015)

**Recently, there has been renewed interest in the coupling between geometry and topological defects in crystalline and striped systems. Standard lore dictates that positive disclinations are associated with positive Gaussian curvature, whereas negative disclinations give rise to negative curvature. Here, we present a diblock copolymer system exhibiting a striped columnar phase that preferentially forms wrinkles perpendicular to the underlying stripes. In free-standing films this wrinkling behavior induces negative Gaussian curvature to form in the vicinity of positive disclinations.**

disclinations and curvature | diblock copolymer | smectic | free-standing membrane | wrinkling instability

Non-Euclidean geometry has been shown to be one of the most robust mechanisms used to prescribe the configuration of defects in crystalline (1, 2) or striped phases (3–5). Gaussian curvature can also stabilize more exotic defects, including scars (6), fractionalized defect charges (7), and pleats (8). Likewise, if a 2D crystal is allowed to buckle out of the plane, the elastic energy associated with isolated disclinations can be strongly reduced by screening their strain fields through curvature, trading off stretching for bending energy (9, 10). Depending on the sign of the topological charge, isolated defects can deform the membrane into cone- or saddle-shape configurations, acting as sources of Gaussian curvature (9, 11). Here we demonstrate experimentally, theoretically, and through simulations that the molecular splay distortions associated with disclinations in a free-standing smectic membrane act as sources of Gaussian curvature, resulting in a pattern of wrinkles in the membrane that form perpendicular to the underlying smectic layers. Dramatically, wrinkling changes the very nature of the curvature-defect coupling, making positive disclinations sources of negative curvature in contrast to intuition gained from geodesic domes and soccer balls. By dictating the distribution of topological defects, it should be possible to control the specific non-Euclidean geometry of the membrane.

The mechanical anisotropy of striped phases can give the bulk material markedly different properties, depending on the relative orientation of the stiffer direction with respect to the underlying stripes. Although the case in which both the stiffer direction and the stripes are parallel has been previously studied (3, 4), we turn our attention to the peculiarities of the perpendicular case, in particular the preference of the perturbed system to form wrinkles orthogonal to the stripes. Defects, ubiquitous in 2D systems, also signal locations of ill-defined elasticity and thus function as sources of geometry in a free-standing membrane. We note that purely molecular splay can drive this unusual behavior in nematic elastomers due to anisotropic swelling (12–15). However, the present system relies on wrinkle formation due to anisotropic elastic moduli as a means of coupling curvature to disclinations.

The two main obstacles to studying the coupling between disclinations and elastic deformations are accurately controlling the distribution of disclinations and simultaneously measuring both the height and the smectic phase of a free-standing membrane. Both challenges can be overcome by studying thin films of cylinder-forming block copolymers; a monolayer of cylinders behaves as a 2D smectic, wherein the density of defects can be controlled quite easily through coarsening. At a constant temperature above the glass transition temperature ($T_g$) of both blocks, the average distance between disclinations measured by the orientational correlation length $\xi_2$ scales with time as $\xi_2 \sim t^{1/4}$ (16). In particular, we consider the cylinder-forming block copolymer polystyrene-block-poly(ethylene-alt-propylene) (PS-PEP). This polymer was chosen in part for its thermal properties, as room temperature is below the $T_g$ of the polystyrene (PS) block and above the $T_g$ of the poly(ethylene-alt-propylene) (PEP) block. The difference between the moduli of the glassy PS cylinders and the rubbery PEP matrix gives rise to a strong contrast in atomic force microscopy (AFM) images.

Spin coating a thin layer of polymer on a dissolvable surface ensured a uniform monolayer of cylinders. After thermally annealing the membrane to achieve the desired defect density, the samples were quenched to room temperature, arresting any coarsening. By carefully immersing the sample in water, the membrane cleanly separated from the substrate. The freely floating film was captured on a transmission electron microscopy (TEM) grid and viewed through AFM, where height fluctuations and smectic phase could be measured simultaneously (Fig. 1*A*). All measurements were in a regime where the TEM grid spacing 25 μm $\gg \xi_2 > d_{sm} = 21$ nm, where $d_{sm}$ is the center to center spacing of the cylinders in the diblock. Upon being released from the flat substrate, the free-standing membrane buckled. The resulting surface consisted of

## Significance

**Diblock copolymers, polymers made by covalently bonding two otherwise immiscible polymers together, are prized for their robust ability to self-assemble into highly ordered geometric structures. Likewise, there has been recent interest in the ability to control the global geometry of a surface, merely by modifying its local microstructure. Here, we take advantage of the defect structure arising from a slow annealing of a thin film of cylinder-forming diblock copolymers as a means of guiding the geometry of an emergent three-dimensional structure.**

Author contributions: D.A.V., P.M.C., and R.A.R. designed research; E.A.M., D.A.V., A.D.P., and N.A.G. performed research; E.A.M. analyzed data; E.A.M. and D.A.V. wrote the paper; E.A.M. designed the theory; D.A.V. performed simulations; and A.D.P. performed simulations and designed theory.

The authors declare no conflict of interest.

This article is a PNAS Direct Submission.

[1]E.A.M. and D.A.V. contributed equally to this work.

[2]To whom correspondence may be addressed. Email: sabetta.matsumoto@gmail.com or dvega@criba.edu.ar.

[3]Present address: Consiglio Nazionale delle Ricerche-Istituto dei Sistemi Complessi and Dipartimento di Fisica, Università di Roma La Sapienza, 00185 Rome, Italy.

This article contains supporting information online at www.pnas.org/lookup/suppl/doi:10.1073/pnas.1514379112/-/DCSupplemental.

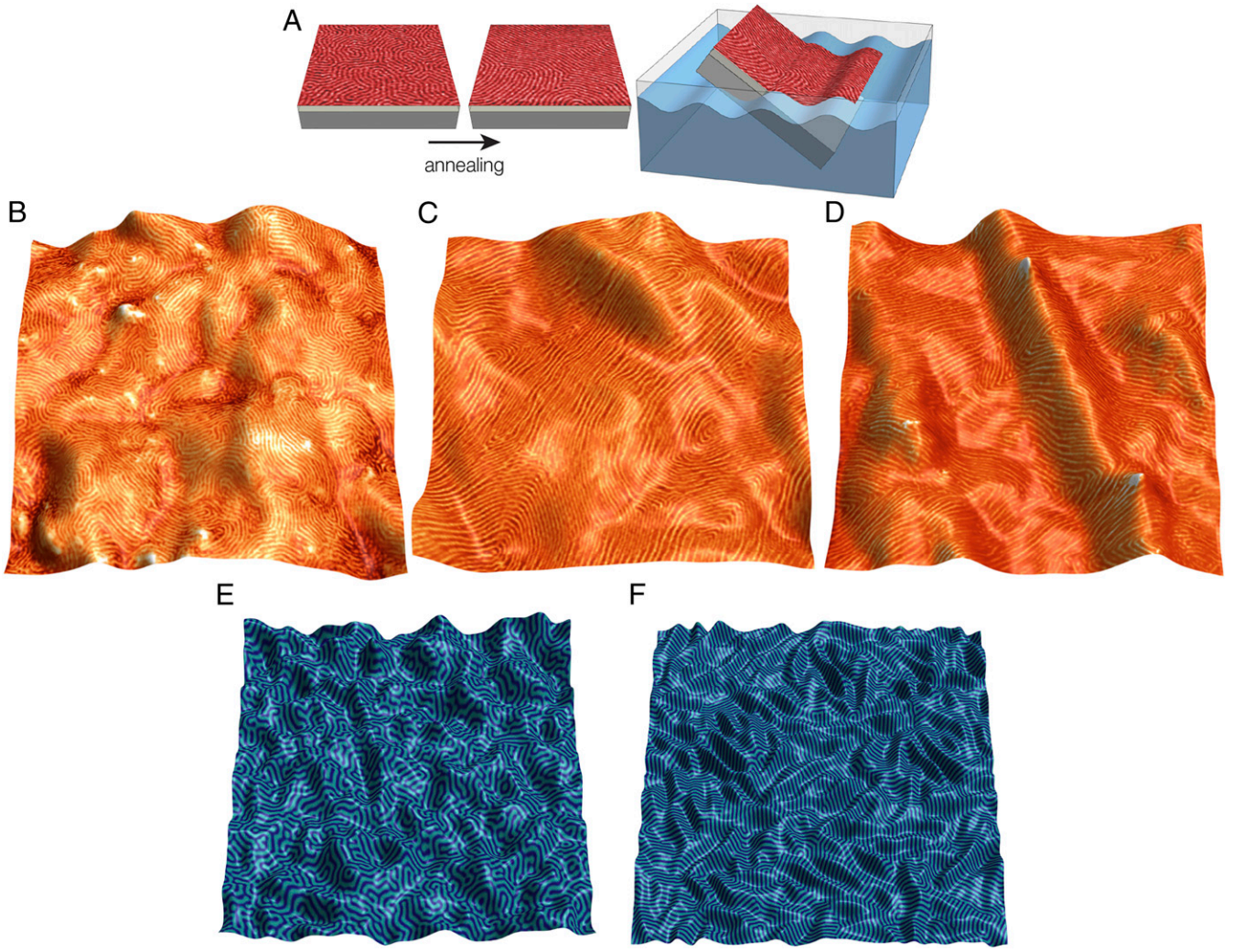


**Fig. 1.** (*A*) Schematic showing the preparation of freestanding smectic membranes. A 30-nm layer of cylinder-forming PS-PEP was deposited on a 50-nm layer of sucrose. The monolayer of cylinders coarsens according to the law $\xi_2 \sim t^{1/4}$ at 363 K to achieve the desired density of defects. After the membrane is released from the substrate, it is captured on a TEM grid. (*B–D*) AFM images of the freestanding films simultaneously measure height and the location of the cylinders. Three samples with orientational correlation lengths $\xi_2 = 42$ nm (*B*) $\xi_2 = 217$ nm (*C*), and $\xi_2 = 244$ nm (*D*) show the coupling between the smectic order and the membrane geometry. The coloration of each of the (2 μm)$^2$ images indicates the local smectic layers. (*E* and *F*) Likewise, two simulated membranes with (*E*) $\xi_2 = 11$ nm and (*F*) $\xi_2 = 67$ nm have average wrinkle wavelengths of 206 nm and 203 nm, respectively. The simulated membranes are calibrated such that the average smectic layer spacing $d_{sm} = 21$ nm matches the experimentally determined value.

wrinkles with a well-defined wavelength. Multiple scans of each film ensured that neither thermal fluctuations nor hydration gradients were responsible for the wrinkles. To study the coupling between smectic order and the membrane topography, membranes were fabricated with $\xi_2$ spanning nearly an order of magnitude, from 42 nm to 244 nm (Fig. 1 *B–D* and Fig. S1).

In concert with the experimental system, we use a simple model to explore the effects of in-plane elastic stresses due to topological defects on the geometry of the membrane. Combining the Helfrich–Canham model of a fluid membrane and the classical Brazovskii model describing striped phases accounts for both smectic order and membrane elasticity (11). The equilibrium configuration of unstructured fluid membranes has been extensively studied since the pioneering papers by Helfrich (17) and Canham (18). According to the Helfrich–Canham theory (10, 19, 20), the membrane free energy can be described by

$$F_{\mathrm{HC}} = \int \sqrt{g} d^2x \left[ \frac{k_b}{2} H^2 + \frac{k_g}{2} K + \sigma \right], \qquad [1]$$

where $g$ is the metric tensor, $H$ and $K$ are respectively the mean and Gaussian curvatures, $k_b$ and $k_g$ are bending modulus and Gaussian rigidity, respectively, and $\sigma$ is the constant surface tension. Although the Gaussian curvature term is normally ignored as a purely topological term, the free boundaries in these membranes allow for varying amounts of Gaussian curvature to be expressed. Likewise, the ordered structure of diblock copolymers can be described to first order by a Brazovskii model that accounts for long- and short-ranged interactions (21). Taking into account the membrane geometry, the Brazovskii free energy for a striped diblock copolymer is given by

$$F_{\mathrm{B}} = \int \sqrt{g} d^2x \left[ 2\left(\nabla^2_{\mathrm{LB}}\psi\right)^2 - 2\nabla_i\psi\nabla^i\psi + \frac{t}{2}\psi^2 + \frac{1}{4}\psi^4 \right], \qquad [2]$$

where $\psi(\mathbf{r})$ is the smectic order parameter, $g$ is the metric of the membrane, $t = (T_c - T)/T_c$ is the reduced temperature, with $T_c$ denoting the critical temperature, and the coupling between membrane shape and smectic order parameter enters through the metric of the membrane and the Laplace–Beltrami operator $\nabla^2_{\mathrm{LB}} = (1/\sqrt{g})\partial_i \sqrt{g} g^{ij} \partial_j$ (22). Here we use the standard summation index

convention. At low temperatures, $F_B$ favors the formation of the smectic phase with a well-defined wavevector $k_0 = 1/\sqrt{2}$. A linear instability analysis relates the Brazovskii free energy to the standard smectic free energy, $F_{sm} = (1/2)\int d^3x[B(1-(\nabla\phi)^2) + K_1(\nabla\cdot\mathbf{n})^2]$, where the smectic layers are defined by level sets of the phase field $\phi(\mathbf{r}) = nd$, $n \in \mathbb{Z}$, the in-plane director field is given by $\mathbf{n} = \nabla\phi/|\nabla\phi|$, and $B$ and $K_1$ are respectively the compression modulus and splay constant. Both smectic elastic constants can be written as functions of the reduced temperature (*SI Text* and ref. 23). Adding fluid membrane and smectic contributions to the free energy, we arrive at the final Hamiltonian: $F_{\psi,h} = F_{HC} + F_B$.

In addition to the analytic treatment of the static equations, we also study the coupling between membrane geometry and smectic order by numerically solving the dynamical model

$$\frac{\partial\psi}{\partial t} = -\nabla^2_{LB}\left[\frac{\partial F_{\psi,h}}{\partial\psi}\right] + \eta_\psi(\mathbf{r},t), \quad \frac{\partial h}{\partial t} = -\frac{\partial F_{\psi,h}}{\partial h} + \eta_h(\mathbf{r},t), \qquad [3]$$

where $\eta_\psi(\mathbf{r},t)$ and $\eta_h(\mathbf{r},t)$ are random Gaussian noise fields satisfying the fluctuation dissipation theorem (11). As in the experiment, $\psi(\mathbf{r},t)$ is first evaluated in a planar system ($h = 0$) to obtain the desired defect density. Immediately following a quench below

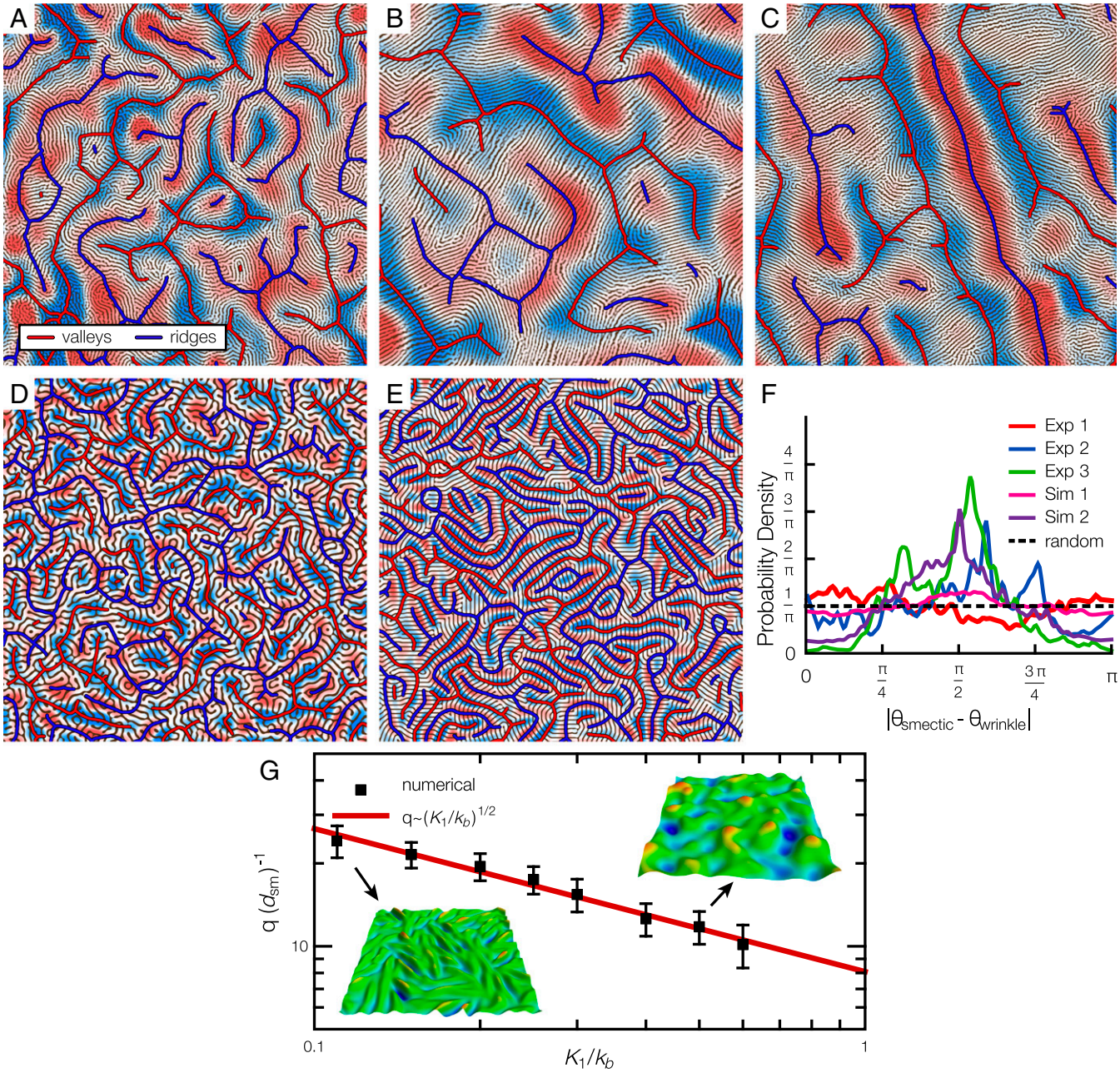


**Fig. 2.** (*A–E*) The peaks (red) and valleys (blue) of wrinkles with relation to the underlying smectic order. As $\xi_2$ increases, the wrinkles and smectic layers become more perpendicular. The membrane with the smallest $\xi_2 = 42$ nm (*A*) has a wavelength of $\lambda = 385$ nm, whereas the membranes with larger correlation lengths, $\xi_2 = 217$ nm (*B*) and $\xi_2 = 244$ nm (*C*), both have a wavelength of $\lambda \approx 593$ nm. (*D*) Similarly, the simulated membrane with $\xi_2 = 11$ nm has an average wrinkle wavelength of 206 nm. The wrinkles are quite disordered on the length scale of the smectic order. (*E*) In the opposite limit, the orientational correlation length is much greater than the block copolymer period, $\xi_2 = 67$ nm $\gg d_{sm} = 21$ nm. (*F*) The tendency for the wrinkles to align perpendicular to the smectic with increasing $\xi_2$ can be seen in this histogram. (*G*) In these membranes, the wrinkle wavelength $q = 2\pi/\lambda \sim \sqrt{K_1/k_b}$ scales as the square root of the ratio between the splay $K_1$ and bend $k_b$ elastic constants.

$T_c$, the equilibrium configurations of $h(\mathbf{r},t)$ and $\psi(\mathbf{r},t)$ are calculated. Here, we analyze the results from two simulated membranes with orientational correlation lengths $\xi_2 = 11$ nm (Fig. 1*E*) and $\xi_2 = 67$ nm (Fig. 1*F*).

There are two distinctly different regimes of membrane behavior, depending on the orientational correlation length or, equivalently, the average distance between defects. In the membrane with the smallest orientational correlation length $\xi_2 = 42$ nm, the wrinkles have an average wavelength of $\lambda = 385$ nm, and they appear to be quite disordered (Fig. 2*A*). In the membranes with much larger values of $\xi_2$, not only does the wavelength change, but also the coupling between the in-plane smectic order and large-scale membrane deformations begins to show up. One might expect the elastic anisotropy due to the difference between cylinders and matrix to penalize bending along the cylinders, causing the wrinkles to form parallel to the underlying smectic layers (3, 4). However, the wrinkles are perpendicular to the smectic in membranes with $\xi_2$ ranging from 217 nm to 244 nm. Remarkably, they all have the same wavelength of $\lambda \approx 593 \pm 6$ nm (Fig. 2 *B* and *C*, Table S1, and Fig. S2). Increasing $\xi_2$ results in surfaces with more uniform and ordered wrinkles.

Numerical minimization of Eq. **3** faithfully reproduces many features of the experimental membranes. In both types of membranes, changing the density of defects affects the order and regularity of the wrinkle patterns. When $\xi_2 \ll \lambda$, within each wavelength the disorder coming from multiple disclinations leads to a disorganized pattern of bumps and wrinkles (Fig. 2 *A* and *D*). In effect, the system behaves as an unstructured membrane, where there is quenched disorder associated with the overlapping distortion fields coming from each defect. Whereas for values of $\xi_2 \gtrsim \lambda$ the wrinkles become well organized and orient perpendicular to the smectic layers (Fig. 2 *B*, *C*, *E*, and *F* and Fig. S2). Because the numerical model explores a much broader range of ratios $\xi_2/\lambda$ than the experiment, the coupling between curvature and disclinations can be more easily unveiled. The numerical model can also probe the effects of different elastic constants. Fig. 2*G* shows the dominant wavevector $q = 2\pi/\lambda$ of each wrinkle as a function of the ratio of the splay $K_1$ and bend $k_b$ elastic constants.

To understand the interplay between smectic orientation and wavelength, let us, for simplicity, consider a single, isolated +1 disclination described by $\psi = a\cos(qr)$ or $\phi = r$ located at the center of a circular membrane. (Although +1 disclinations are rarely, if ever, seen in experiment, a $+(1/2)$ disclination consists of a half-plane of the +1 disclination attached to a half-plane containing an ideal flat smectic.) Here, the elastic distortions involve only splay contributions. Thus, to leading order the Brazovskii and smectic free energies are identical. For ease of computation, we use the smectic free energy. The flat system has a splay energy $F_{\text{splay}} = (K_1/2)\int d^2x(\nabla\cdot\hat{\mathbf{r}})^2 = (K_1/2)\int_0^{2\pi} d\theta \int_a^R dr/r = (K_1/2)\ln(R/a)$, where $R$ is the system size and $a$ is the size of the defect core.

Upon buckling, the metric of the surface becomes non-Euclidean, affecting both the splay energy of the smectic and the bending energy of the membrane. To estimate the role of the different free energy contributions, we consider the membrane geometry in cylindrical Monge gauge, $X(r,\theta) = \{r\cos(\theta),\ r\sin(\theta),\ h(r,\theta)\}$, which has the metric $\sqrt{g} = (r^2 + (\nabla h)^2)^{1/2}$. We assume that the surface is slowly varying or $\nabla h$ is small. $h(r,\theta) = h_0\cos(n\theta)$, where the maximum height of the distortions $h_0$ and the wavelength at radius $r_0$ are $\lambda = 2\pi r_0/n = qr_0$. This surface deformation has a nonzero energy due to contributions from both mean curvature, $F_{\text{bend}} \approx (k_b/2)\int d^2x\sqrt{g}((1/2)\nabla^2 h)^2 \approx (\pi k_b/8)\int dr(h_0^2 n^4/r^3)$, and surface area, $F_\sigma = 2\sigma\int d^2x\sqrt{g} \approx 2\pi\sigma\int dr(1 + h_0^2 n^2/4r^2)$, whereas Gaussian curvature away from the disclination core remains zero. However, the surface deformation also lowers the splay energy, because splay measures the divergence of the average molecular orientation. The smectic energy can be approximated as $F_{\text{splay}} = (K_1/2)\int d^2x\sqrt{g}(g^{-1/2}\partial_i(\sqrt{g}n^i))^2 \approx \pi K_1\int dr(1/r)(1 - 3h_0^2 n^2/4r^2)$. Thus, adding the three terms of the energy and minimizing with regard to $n$ produce

$$qr \sim \sqrt{\frac{3K_1 - 4\sigma r^2}{k_b}}. \qquad [4]$$

For elastic constants given by $k_b \sim 1.7\times10^{-8}$ erg, $K_1 \sim 4.6\times10^{-8}$ erg, and $\sigma \sim 30.6$ dyn·cm$^{-1}$ (*SI Text*), the estimated wavelength for $r = \xi_2 = 217$ nm, $\lambda \sim 627$ nm, is found to be in agreement with the experimental measurements. Further experiments with many different polymers would be needed to examine this degree of freedom.

Because disclinations are points where the local smectic orientation winds by $m\pi/2$, $m \in \mathbb{Z} \leq 2$, they facilitate bending or branching of the wrinkles. Isolated $+(1/2)$ disclinations, places where radially oriented wrinkles meet, are therefore centers of negative Gaussian curvature, and conversely, $-(1/2)$ disclinations, which allow wrinkles to bend, are centers of positive Gaussian curvature. To elucidate this unexpected wrinkle-driven coupling between disclinations and curvature, let us consider two ideal cases: the +1 disclination and the $-(1/2)$ disclination. Surfaces can be constructed from waves with normals to the wavefront taken from the in-plane tangents to the local smectic layers and phase offset chosen such that the height is given by a $C^2$ function. Upon calculating the Gaussian curvatures of both surfaces, it becomes evident that the positive and negative disclinations must be centers of negative and positive curvature, respectively (Fig. 3).

The correlation between defect density and wrinkle organization extends to curvature, as the orientation of the wrinkles dictates the local sign of Gaussian curvature. The crossover in behavior occurs when the orientational correlation length exceeds half the elastic wrinkle wavelength, $\xi_2 \gtrsim \lambda/2$. At this length scale, a single disclination can have influence over the wrinkles surrounding it, without the influence of neighboring disclinations. The more ordered a membrane is, the stronger the preference for large negative

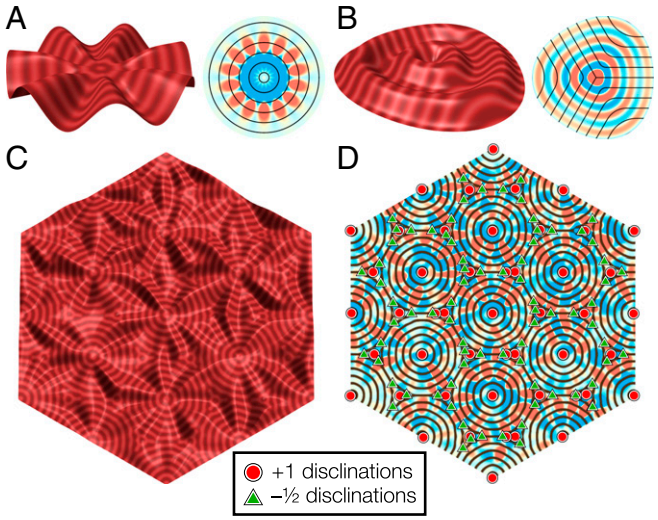


**Fig. 3.** (*A* and *B*) Schematic illustrating the relationship between wrinkles and Gaussian curvature in (*A*) +1 and (*B*) $-(1/2)$ disclinations. Wrinkles are constructed such that they are everywhere perpendicular to the smectic order. The Gaussian curvature for both of these structures demonstrates that +1 ($-(1/2)$) disclinations are centers of negative (positive) curvature, where $K > 0$ ($K < 0$) is shown in orange (blue). (*C*) Complex membrane topographies can be generated merely by choosing the locations of disclinations, as demonstrated in this simulation. (*D*) +1 (red circles) and $-(1/2)$ (green triangles) disclinations have average values of Gaussian curvature $-3 \pm 5\times10^{-7}(d_{\text{sm}})^2$ and $0.4 \pm 5\times10^{-7}(d_{\text{sm}})^2$, respectively.

(positive) values of curvature associated with $+(1/2)$ $(-(1/2))$ disclinations (Fig. 4 *A*–*E* and Fig. S3). Note that this tendency is stronger for positive disclinations, as more than 71% of $+(1/2)$ disclinations are sources of negative Gaussian curvature (Fig. 4 *F* and *G* and Table S2). Positive disclinations give splay to the wrinkles, thereby accommodating more area than an equivalent flat membrane.

In summary, we have found that topological defects can induce wrinkling in smectic membranes. The wrinkles in the membrane reveal not only the nature of the stress field associated with the defects, but also the anisotropic behavior of the smectic phase. Unlike crystalline systems, $+(1/2)$ $(-(1/2))$ disclinations are centers of negative (positive) Gaussian curvature. The simple relationship between elastic constants and wrinkle wavelength provides a method to characterize the properties of multicomponent, anisotropic thin films. Whereas defect-induced deformations have been experimentally observed in different systems, including graphene (24, 25) and lyotropic gels (26), it is hoped that this work will stimulate further experimental research to study the process of wrinkling in different textured

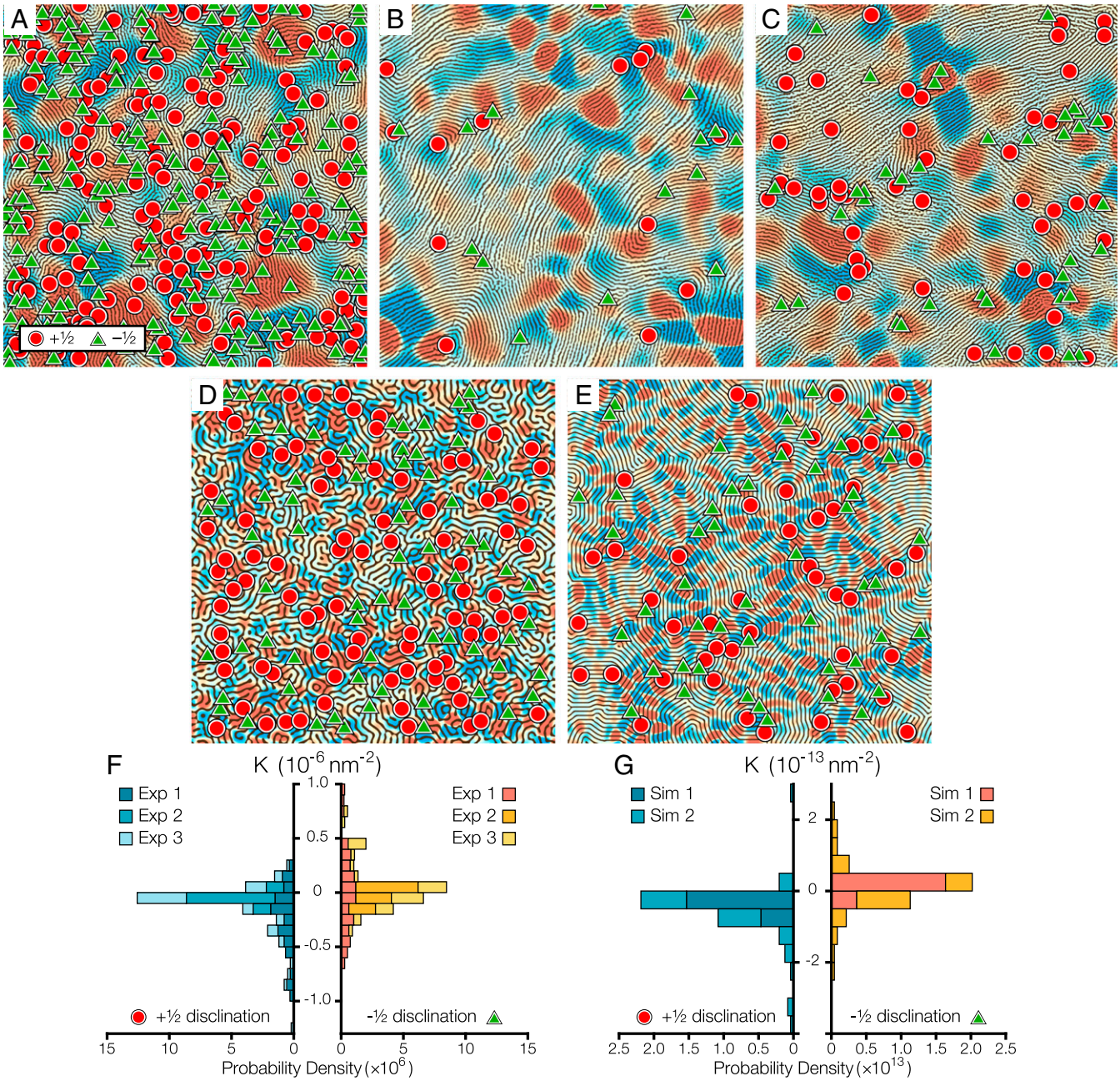


**Fig. 4.** Surfaces are colored by mean curvature where $H > 0$ ($H < 0$) is shown in red (blue). (*A*–*E*) Isolated $+(1/2)$ $(-(1/2))$ disclinations, depicted by red circles (green triangles), are shown with respect to the Gaussian curvature. In the regime where $\xi_2 \ll \lambda/2$, the experimental membrane (*A*) and the simulated membrane (*D*) display little correlation between the locations of the disclinations and their associated Gaussian curvatures. In the opposite limit, where $\xi_2 \gtrsim \lambda/2$, more than 71% of $+(1/2)$ disclinations are located at negatively curved parts of the membrane in two experimental membranes (*B* and *C*) and a simulated membrane (*E*). (*F* and *G*) Histograms of the Gaussian curvature for each type of defect show a strong correlation between the sign of the disclination and curvature of the opposite sign for both experimental (*F*) and simulated (*G*) membranes.

membranes. Our findings can have important implications in the use of smectic membranes as actuators or in the development of novel defect-prescribed shapes.

## Materials and Methods

**Synthesizing Polymer.** The smectic membranes consist of a free-standing thin film made of a cylinder-forming PS-PEP diblock copolymer. The block copolymer was synthesized through sequential living anionic polymerization of styrene and isoprene followed by selective saturation of the isoprene block (see ref. 27 for more details). The number-average block molecular weights for the block copolymer are 4.3 kg/mol for PS and 13.2 kg/mol for PEP. The bulk morphology of the block copolymer consists of hexagonally packed PS cylinders embedded in the PEP matrix. For this system the glass transition temperature for the PS block is about 330 K, whereas the order–disorder transition temperature is $T_{ODT} = 417$ K (the glass transition temperature of the PEP block is well below room temperature). In thin films, the cylinders adopt a configuration parallel to the substrate because of large surface energy differences between the blocks. The repeat spacing for the block copolymer is 21 nm (measured on thin films by AFM).

**Creating the Freestanding Membranes.** To obtain the freestanding membrane a monolayer of block copolymer was spin coated onto a 50-nm-thick flat layer of sucrose deposited onto a silicon wafer. The 50-nm-thick sucrose films were prepared via spin coating from a 3 wt% solution in water. The block copolymer thin films were prepared via spin coating from a 1 wt% solution in toluene, a good solvent for both blocks. By manipulating the spin speed, the thickness of the film, measured through ellipsometry, can be controlled. We produced a monolayer of cylinders, plus the associated brush-like wetting layer at the substrate (~30-nm-thick film of PS-PEP 4/13). Order was induced through annealing at $T = 363$ K, above the glass transition of the PS block and below the $T_{ODT}$ of the block copolymer (28). During this process the content of defects is strongly reduced and the degree of order in the pattern is mainly disrupted by $\pm 1/2$ disclination multipoles (28). After annealing, the film was lifted off the substrate and deposited on a TEM grid. To analyze the effect of the liftoff procedure in water, test samples were redeposited onto a silicon wafer. Because the process occurs at room temperature, well below the glass transition temperature of the minority block in the copolymer, it was found that the individual layers retain the symmetry, average intercylinder distance, and structure established during the annealing. The thin films were imaged using a Bruker Dimension 3000 AFM in tapping mode. The spring constant of the tip (uncoated Si) was ~40 N/m and its resonant frequency was 300 kHz.

**ACKNOWLEDGMENTS.** We gratefully acknowledge helpful discussions with B. Davidovitch; Douglas Adamson for the synthesis of the PS-PEP 4/13; and the financial support from the National Science Foundation (NSF) MRSEC Program through the Princeton Center for Complex Materials (DMR-0819860 and DMR-1420541), the NSF Materials Research Science and Engineering Center (MRSEC) Program through the Harvard Paulson School of Engineering and Applied Sciences (DMR-0820484), NSF Grant DMR-1105417, the Princeton Center for Theoretical Science, Universidad Nacional del Sur, and the National Research Council of Argentina (CONICET).

1. Bowick MJ, Nelson DR, Travesset A (2000) Interacting topological defects on frozen topographies. *Phys Rev B* 62(13):8738–8751.
2. Bowick MJ, Giomi L (2009) Two-dimensional matter: Order, curvature and defects. *Adv Phys* 58(5):449–563.
3. Santangelo CD, Vitelli V, Kamien RD, Nelson DR (2007) Geometric theory of columnar phases on curved substrates. *Phys Rev Lett* 99(1):017801.
4. Kamien RD, Nelson DR, Santangelo CD, Vitelli V (2009) Extrinsic curvature, geometric optics, and lamellar order on curved substrates. *Phys Rev E Stat Nonlin Soft Matter Phys* 80(5 Pt 1):051703.
5. Gómez LR, Vega DA (2009) Relaxational dynamics of smectic phases on a curved substrate. *Phys Rev E Stat Nonlin Soft Matter Phys* 79(3 Pt 1):031701.
6. Bausch AR, et al. (2003) Grain boundary scars and spherical crystallography. *Science* 299(5613):1716–1718.
7. Irvine WTM, Vitelli V, Chaikin PM (2010) Pleats in crystals on curved surfaces. *Nature* 468(7326):947–951.
8. Irvine WTM, Bowick MJ, Chaikin PM (2012) Fractionalization of interstitials in curved colloidal crystals. *Nat Mater* 11(11):948–951.
9. Seung HS, Nelson DR (1988) Defects in flexible membranes with crystalline order. *Phys Rev A* 38(2):1005–1018.
10. Park JM, Lubensky TC (1996) Disclination asymmetry in deformable hexatic membranes and the Kosterlitz-Thouless transitions. *J Phys I France* 6(4):493–502.
11. Pezzutti AD, Vega DA (2011) Defect dynamics in crystalline buckled membranes. *Phys Rev E Stat Nonlin Soft Matter Phys* 84(1 Pt 1):011123.
12. Modes CD, Bhattacharya K, Warner M (2010) Disclination-mediated thermo-optical response in nematic glass sheets. *Phys Rev E Stat Nonlin Soft Matter Phys* 81(6 Pt 1): 060701.
13. Modes CD, Bhattacharya K, Warner M (2011) Gaussian curvature from flat elastica sheets. *Proc R Soc A* 467(2128):1121–1140.
14. de Haan LT, Sánchez-Somolinos C, Bastiaansen CM, Schenning AP, Broer DJ (2012) Engineering of complex order and the macroscopic deformation of liquid crystal polymer networks. *Angew Chem Int Ed Engl* 51(50):12469–12472.
15. McConney ME, et al. (2013) Topography from topology: Photoinduced surface features generated in liquid crystal polymer networks. *Adv Mater* 25(41):5880–5885.
16. Harrison C, et al. (2000) Mechanisms of ordering in striped patterns. *Science* 290(5496):1558–1560.
17. Helfrich W (1973) Elastic properties of lipid bilayers: Theory and possible experiments. *Z Naturforsch C* 28(11):693–703.
18. Canham PB (1970) The minimum energy of bending as a possible explanation of the biconcave shape of the human red blood cell. *J Theor Biol* 26(1):61–81.
19. Park JM, Lubensky TC (1996) Topological defects on fluctuating surfaces: General properties and the Kosterlitz-Thouless transition. *Phys Rev E Stat Phys Plasmas Fluids Relat Interdiscip Topics* 53(3):2648–2664.
20. Funkhouser CM, Solis FJ, Thornton K (2007) Coupled composition-deformation phase-field method for multicomponent lipid membranes. *Phys Rev E Stat Nonlin Soft Matter Phys* 76(1 Pt 1):011912.
21. Yamada K, Komura S (2008) The dynamics of order-order phase separation. *J Phys Condens Matter* 20(15):155107.
22. Nelson DR (2002) *Defects and Geometry in Condensed Matter Physics* (Cambridge Univ Press, Cambridge, UK).
23. Amundson K, Helfand E (1993) Quasi-static mechanical properties of lamellar block copolymer microstructure. *Macromolecules* 26(6):1325–1332.
24. Yazyev OV, Louie SG (2010) Electronic transport in polycrystalline graphene. *Nat Mater* 9(10):806–809.
25. Warner JH, et al. (2013) Rippling graphene at the nanoscale through dislocation addition. *Nano Lett* 13(10):4937–4944.
26. Islam MF, Nobili M, Ye F, Lubensky TC, Yodh AG (2005) Cracks and topological defects in lyotropic nematic gels. *Phys Rev Lett* 95(14):148301.
27. Marencic AP, Adamson DH, Chaikin PM, Register RA (2010) Shear alignment and realignment of sphere-forming and cylinder-forming block-copolymer thin films. *Phys Rev E Stat Nonlin Soft Matter Phys* 81(1 Pt 1):011503.
28. Harrison C, et al. (2002) Dynamics of pattern coarsening in a two-dimensional smectic system. *Phys Rev E Stat Nonlin Soft Matter Phys* 66(1 Pt 1):011706.